Available online at www.sciencedirect.com
SCIENCE DIRECT®
Journal of Computational Physics 200 (2004) 769–794
JOURNAL OF COMPUTATIONAL PHYSICS
www.elsevier.com/locate/jcp

Adjoint and defect error bounding and correction for functional estimates

Niles A. Pierce [a,*], Michael B. Giles [b]

[a] *Applied & Computational Mathematics, California Institute of Technology, Mail Code 114-96, Pasadena, CA 91125, USA*
[b] *Computing Laboratory, Oxford University, UK*

Received 21 July 2003; received in revised form 22 December 2003; accepted 2 May 2004
Available online 7 June 2004

Abstract

We present two error estimation approaches for bounding or correcting the error in functional estimates such as lift or drag. Adjoint methods quantify the error in a particular output functional that results from residual errors in approximating the solution to the partial differential equation. Defect methods can be used to bound or reduce the error in the entire solution, with corresponding improvements to functional estimates. Both approaches rely on smooth solution reconstructions and may be used separately or in combination to obtain highly accurate solutions with asymptotically sharp error bounds. The adjoint theory is presented for both smooth and shocked problems; numerical experiments confirm fourth-order error estimates for a pressure integral of shocked quasi-1D Euler flow. By employing defect and adjoint methods together and accounting for errors in approximating the geometry, it is possible to obtain functional estimates that exceed the order of accuracy of the discretization process and the reconstruction approach. Superconvergent drag estimates are obtained for subsonic Euler flow over a lifting airfoil.

AMS: 65G99; 76N15

Keywords: Adjoint; Defect; Error bounding; Error correction; Functionals

1. Introduction

Integrals of solutions to partial differential equations (PDEs) provide crucial feedback on system behavior in many areas of engineering and science. In many settings, integral functional values are the primary quantitative outputs of numerical simulations of PDE solutions. In the field of computational fluid dynamics, lift and drag are computed as surface integrals of pressure and shear forces. The desire for efficient computational algorithms that produce reliable and accurate lift and drag values has motived a great

* Corresponding author.
E-mail addresses: niles@caltech.edu (N.A. Pierce), giles@comlab.ox.ac.uk (M.B. Giles).

0021-9991/$ - see front matter
doi:10.1016/j.jcp.2004.05.001

deal of research during the last several decades. Integral functionals also arise in examining the electrostatic free energy of biomolecules in solvent [1] and in the calculation of radar cross-sections based on electromagnetic scattering [2].

Modern numerical methods for PDEs make it possible to solve nonlinear systems with discontinuous solutions in complicated computational domains. Nonetheless, limited computational resources make it desirable to compute solutions to the minimum allowable accuracy. Supposing that the output of most interest is an integral functional, we arrive at two related challenges. For reliability, it is desirable to compute a bound on the remaining error in the functional. For efficiency, it is advantageous to compute the functional value to a higher order of accuracy than the overall solution on which it is based.

The present work describes two approaches to error bounding and error correction for functional estimates. Depending on the priorities of the engineer or scientist, an estimate of the leading term in the functional error may be used either to provide an asymptotically sharp error bound, or to remove the leading error term and obtain a superconvergent estimate.

The first approach relies on the adjoint or dual PDE, whose solution describes the sensitivity of the functional of interest to residual errors in satisfying the original primal PDE [3–6]. Smooth reconstructions of the primal and dual solutions are employed, so the method is equally applicable to finite difference, finite volume or finite element discretizations. The treatment of problems containing shocks requires careful consideration, as addressed in the present work.

A second approach uses the reconstructed primal solution to drive a defect iteration that improves the accuracy of the underlying base solution [5–11]. The resulting corrected solution can be used to estimate the leading error term in the original functional estimate. In practice, the implementation of the defect and adjoint error corrections are very similar. Both are driven by the residual errors which quantify the extent to which the reconstructed solution does not satisfy the original PDE and its boundary conditions. The adjoint correction compensates for the effect of these residual errors on the output functional, whereas the defect correction corrects the entire flow solution.

The two approaches can also be used in combination to obtain even greater accuracy. It is possible for the resulting order of accuracy to be greater than the accuracy of the reconstruction process. However, to achieve this surprising result it is necessary to account for the geometric errors introduced by reconstruction.

Adjoint sensitivities may also be employed as the basis for optimal adaptive meshing strategies [12–14] that seek to maximize the accuracy of the functional estimate for a given computational cost. The issues of error bounding and adaptive error control have received particular attention in the finite element community [2,15–28], where the use of the adjoint PDE for error analysis was first investigated. The orthogonality properties of most finite element methods ensure that functional estimates are naturally superconvergent. The present approach may be used to enhance the natural finite element superconvergence [4].

The study of error convergence is particularly challenging if the true solution is unknown. To facilitate the study of functional accuracy for interesting physical systems and nontrivial computational domains, we formulate *modified* PDEs by postulating a solution and evaluating the source term that is required to make this the solution of the modified equations. If the postulated solution is close to a solution of the original PDEs, then the source term will be small and the modified problem will exercise the numerical method in a very similar manner to the true physics. In the present work, we describe modified Euler problems for two-dimensional flow in a duct and flow over a lifting Joukowski airfoil. These test cases have been invaluable for debugging error estimation algorithms.

Flows with shocks pose a major challenge to both adjoint calculations and adjoint error estimation. The correct formulation of the inviscid adjoint equations must account for linearized perturbations to the shock location. This approach reveals that the adjoint equations corresponding to the steady quasi-1D Euler equations require an interior boundary condition at the shock location [29]. Numerical results using either

the "continuous" approach (approximating the analytical adjoint equations using numerical smoothing in place of the shock boundary condition) or the "discrete" approach (linearising and transposing the discrete flow equations) yield convergent results [30].

Ulbrich has recently developed the analytical formulation of the adjoint equations for unsteady 1D equations with scalar fluxes, such as Burgers equation [31,32]. In this case, numerical results [33] indicate that the "discrete" adjoint approach does not necessarily yield convergent results, unless one uses numerical dissipation that leads to an increasing smoothing of the shock as the mesh is refined. It seems likely that there will be similar problems with the convergence of solutions to the unsteady quasi-1D adjoint Euler equations and to steady adjoint Euler equations in multiple dimensions, although such convergence errors may be very small for weak shocks.

In addition to these difficulties in calculating adjoint solutions, there is the further problem for adjoint error estimation that any smooth reconstructed solution must necessarily have an $O(1)$ local error near the shock. The residual error is therefore likely to increase without bound as the grid is refined. This behavior undermines the whole basis for adjoint methods, which assume small errors, allowing a linearized treatment for error estimation. Here, we describe a new approach that circumvents these difficulties by approximating the inviscid shock as the limiting structure of a viscous shock. Adjoint error estimates subsequently account for the error introduced by the nonzero viscosity and for the numerical error in approximating the viscous shock.

This work greatly expands on our original publication [4] (which introduced adjoint error correction for bulk functionals of smooth solutions to linear and nonlinear PDEs with homogeneous boundary conditions) by addressing adjoint error bounding, defect error bounding and correction, formulations for inhomogeneous boundary conditions and boundary functionals, treatment of shocks, and implementation for two-dimensional Euler flows. We begin by describing error bounding and correction alternatives using adjoint and defect methods. The approaches are then formulated for linear and nonlinear PDEs with inhomogeneous boundary conditions and bulk and boundary functionals. Additional theory is developed for the treatment of shocks and then numerical demonstrations are provided for smooth and shocked quasi-1D Euler flows, 2D duct flow, and flow over a lifting airfoil.

2. Error bounding and correction

Adjoint and defect methods based on smooth solution reconstructions are employed to bound and correct errors in estimates of integrals functionals. The basic methods and alternatives are now introduced in the simplest scenario of a linear differential equation with homogeneous boundary conditions and a bulk functional.

2.1. Adjoint methods

Consider the linear differential equation

$$Lu = f$$

subject to homogeneous boundary conditions on the domain Ω. Suppose we are interested in evaluating the linear functional (g,u), where $(.,.)$ denotes an integral inner product on Ω. This functional may equivalently be evaluated in the dual form (v,f), where v is the solution to the dual or adjoint PDE

$$L^*v = g,$$

subject to homogeneous adjoint boundary conditions. The equivalence of the primal and dual functional representations follows from the definition of the adjoint operator:

$$(v,f) = (v,Lu) \equiv (L^*v,u) = (g,u).$$

The dual form of the functional indicates that the adjoint solution v represents the sensitivity of the functional to the primal source term f.

Discrete approximate primal and dual solutions, U_h and V_h, are computed on a mesh of average interval h. Smooth reconstructions are then obtained

$$u_h \equiv R_h U_h, \quad v_h \equiv R_h V_h,$$

where R_h is a sufficiently smooth reconstruction operator (e.g. C^2 cubic spline interpolation for PDEs of order at most two). The degree to which these functions do not satisfy the original PDEs can then be quantified by the primal and dual *residual errors* defined by

$$Lu_h - f = L(u_h - u), \quad L^* v_h - g = L^*(v_h - v).$$

Assuming that the underlying physical solution is sufficiently smooth, the anticipated order of convergence for the functional estimate depends on: n, the order of the operator L; p, the order of the discrete solution; r, the order of the reconstruction. Intuitively, the solution and residual errors are expected to satisfy

$$\begin{aligned} &\|u_h - u\|, \quad \|v_h - v\| = \mathrm{O}\big(h^{\min(p,r)}\big), \\ &\|Lu_h - f\|, \quad \|L^* v_h - g\| = \mathrm{O}\big(h^{\min(p,r-n)}\big), \end{aligned} \tag{1}$$

where the n differentiations required to evaluate the residual errors account for their reduced accuracy. In practice, these results may only hold in certain norms.

The error in the functional value based on the reconstructed primal solution may be expressed as

$$(g, u_h) - (g, u) = (g, u_h - u) = (L^* v, u_h - u) = (v, L(u_h - u)) = (v, Lu_h - f).$$

Introducing the reconstructed adjoint solution v_h gives

$$(g, u_h) - (g, u) = (v_h, Lu_h - f) - (v_h - v, Lu_h - f).$$

The first term on the right hand side can be evaluated, since f, u_h and v_h are all known. The second term cannot be evaluated because v is unknown. However, the discretization and reconstruction schemes can be chosen to ensure that the second term is $\mathrm{O}(h^{\min(p,r)})$ smaller than the first. Therefore, the first term may be used as an error bound,

$$|(g, u_h) - (g, u)| \leqslant |(v_h, Lu_h - f)| + |(v_h - v, Lu_h - f)| \tag{2}$$

that is sharp asymptotically as h decreases, but may be violated for finite h. Multiplying the error bound by any constant greater than unity will ensure that it is a valid bound for sufficiently small h, but it is not possible in general to say how small h must be.

Alternatively, the first term can be moved to the left hand side to obtain a more accurate functional estimate

$$\{(g, u_h) - (v_h, Lu_h - f)\} - (g, u) = -(v_h - v, Lu_h - f). \tag{3}$$

As a concrete example, consider a one-dimensional Poisson problem

$$L = L^* = \frac{\mathrm{d}^2}{\mathrm{d}x^2}, \quad f = x^3(1-x)^3, \quad g = \sin \pi x$$

with homogeneous boundary conditions on $x \in [0, 1]$. The problem is discretized using second-order finite differences and the solution is reconstructed using cubic spline interpolation ($n = 2$, $p = 2$, $r = 4$). Integrals are evaluated using 3-point Gauss quadrature.

From estimates (1), the reconstructed primal and dual solutions are $O(h^2)$. Also, the functional estimate (g, u_h) has the same order of accuracy as the primal solution on which it is based. The remainder term in (2) and (3) is of order

$$|(v_h - v, Lu_h - f)| = O\left(h^{\min(2,4)+\min(2,4-2)}\right) = O(h^4).$$

Using adjoint error bounding, we expect a second-order functional estimate with an asymptotically sharp error bound that itself contains a fourth-order error. Alternatively, using adjoint error correction, we expect a fourth-order functional estimate. These two alternatives are illustrated by the numerical results in Fig. 1(a). Lines of slope -2 and -4 are drawn through the error values on the finest mesh to assist in determining the convergence rates. Note that the error bound is indistinguishable from the remaining error, as it is roughly 10^2 times more accurate than the functional estimate on the coarsest mesh, increasing to roughly 10^5 times more accurate on the finest mesh. Using adjoint error correction, rigorous a priori analysis of the errors in the primal and dual numerical solutions as well as the errors associated with the

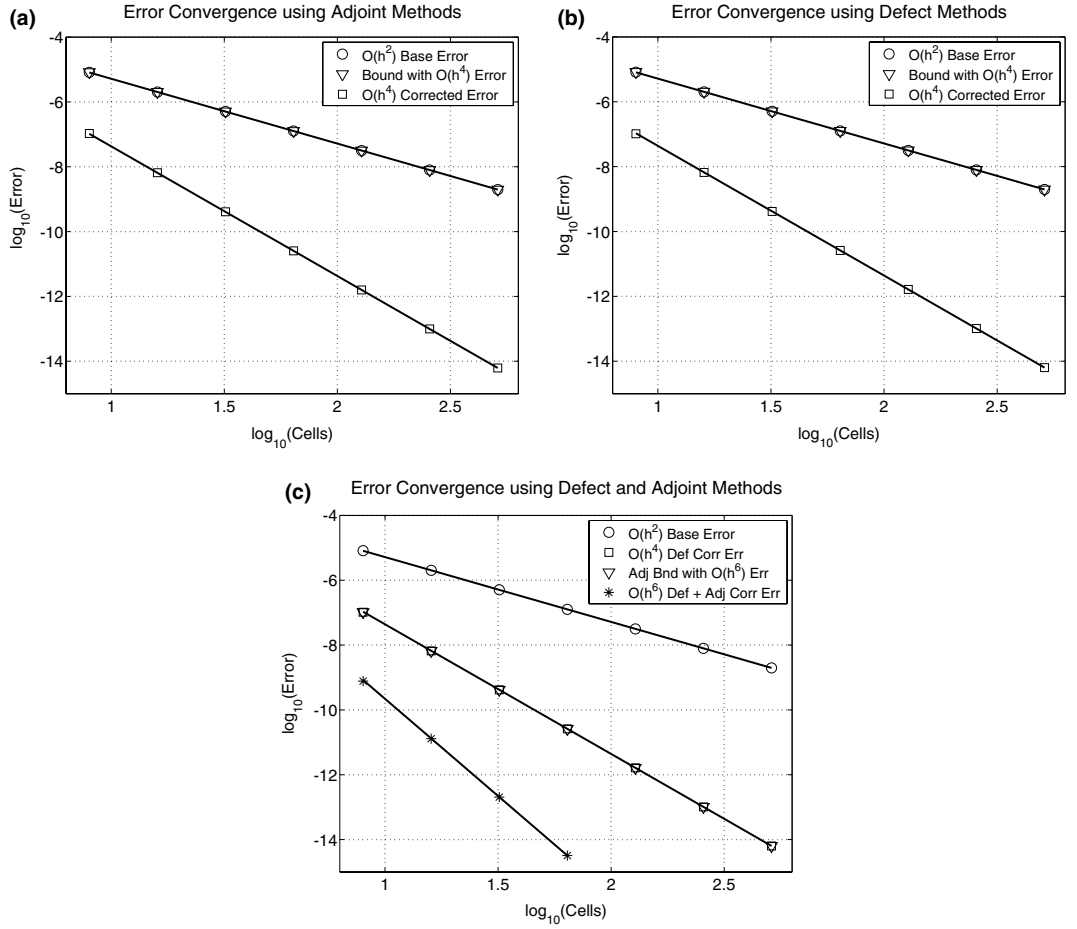

Fig. 1. Functional estimates for a 1D Poisson problem: (a) adjoint error bounding and correction, (b) defect error bounding and correction, (c) defect error correction followed by adjoint error bounding or correction. The superimposed lines have slope -2,-4 or -6 as suggested by the rate descriptions in the legends.

spline reconstruction confirms that the functional accuracy should in fact double from second- to fourth-order [34].

Depending on the reconstruction method, it is possible that the inner product $(v_h - v, Lu_h - f)$ or equivalently $(L^* v_h - g, u_h - u)$ will exhibit a convergence rate that is *faster* than the product of the convergence rates of its components. This results from cancellation effects that have been observed and analyzed in the nonlinear case of smooth quasi-1D Euler flow [34].

2.2. Defect methods

As an alternative to adjoint methods, solution reconstruction may be used to drive a defect correction process [7–10]. If the original numerical solution is obtained by solving the discrete problem

$$L_h U_h = T_h f,$$

where T_h is an operator that transfers the continuous source term f to discrete source terms associated with each of the unknowns in U_h, then the defect correction iteration may be written as

$$\begin{aligned} L_h \Delta U_h &= T_h(f - Lu_h), \\ u_{dh} &= u_h + R_h \Delta U_h, \end{aligned} \tag{4}$$

where R_h is the linear reconstruction operator [5,11]. Note that this defect correction procedure differs from familiar defect correction approaches [35–41] that evaluate Lu_h using a higher order discrete operator L'_h applied to the low order solution U_h (instead of the differential operator L applied to the reconstructed solution u_h). If the defect iteration is convergent, the final accuracy of the defect corrected approximate solution u_{dh} is determined *not* by the low order discrete operator L_h used to obtain the solution, but instead by the interpolation accuracy of the reconstruction method used to form u_h and u_{dh}. See [42] for an overview of defect correction methods and related analysis concerning accuracy, stability and convergence of defect iterations.

Using the reconstructed defect solution u_{dh}, the error in the original functional estimate may be represented

$$(g, u_h) - (g, u) = (g, u_h - u_{dh}) + (g, u_{dh} - u),$$

where the first term on the right-hand side may be evaluated to provide an asymptotically sharp error bound

$$|(g, u_h) - (g, u)| \leqslant |(g, u_h - u_{dh})| + |(g, u_{dh} - u)|,$$

or subtracted to give a more accurate functional estimate

$$\{(g, u_h) - (g, u_h - u_{dh})\} - (g, u) = (g, u_{dh} - u). \tag{5}$$

For the previously considered 1D Poisson problem, defect correction of the primal solution using cubic spline reconstruction yields fourth-order solution errors and consequently a fourth-order functional estimate. The behavior for error bounding and correction is illustrated in Fig. 1(b).

2.3. Combined adjoint and defect methods

Combined approaches yield even sharper error estimates. The remaining error in (5) may be expressed in the dual form

$$(g, u_{dh}) - (g, u) = (g, u_{dh} - u) = (L^* v, u_{dh} - u) = (v, L(u_{dh} - u)) = (v, Lu_{dh} - f).$$

We introduce the reconstructed dual solution v_h,

$$(g, u_{dh}) - (g, u) = (v_h, Lu_{dh} - f) - (v_h - v, Lu_{dh} - f),$$

and evaluate the first term on the right-hand side to obtain either the asymptotically sharp error bound

$$|(g, u_{dh}) - (g, u)| \leqslant |(v_h, Lu_{dh} - f)| + |(v_h - v, Lu_{dh} - f)|$$

or the more accurate functional estimate

$$\{(g, u_{dh}) - (v_h, Lu_{dh} - f)\} - (g, u) = -(v_h - v, Lu_{dh} - f) = -(L^* v_h - g, u_{dh} - u). \tag{6}$$

For the 1D Poisson problem, the order of the remainder term may be estimated as

$$|(L^* v_h - g, u_{dh} - u)| = \mathrm{O}\big(h^{\min(2,4-2)+\min(4,4)}\big) = \mathrm{O}(h^6).$$

Note that an estimate based on the alternative dual representation of the remainder in (6) would appear to be only $\mathrm{O}(h^4)$. Integration by parts to obtain the primal form shows that this estimate is overly pessimistic. Hence, in the numerical results of Fig. 1(c), we observe either a fourth-order functional estimate with a sharp error bound that itself contains a sixth-order error, or else a sixth-order functional estimate without a computable bound.

3. Linear formulation

3.1. Adjoint error estimates

We now extend the adjoint error estimation approach to problems with inhomogeneous boundary conditions and output functionals that contain boundary integrals [3,5].

Let u be the solution of the linear differential equation

$$Lu = f,$$

in the domain Ω, subject to the linear boundary conditions

$$Bu = e,$$

on the boundary $\partial\Omega$. In general, the number of boundary conditions described by the operator B may be different on different parts of the boundary (e.g. inflow and outflow sections for hyperbolic problems).

The output functional of interest contains both bulk and boundary contributions

$$J = (g, u) + (h, Cu)_{\partial\Omega},$$

where $(.,.)_{\partial\Omega}$ represents an integral inner product over the boundary $\partial\Omega$. The boundary operator C may be algebraic (e.g. $Cu \equiv u$) or differential (e.g. $Cu \equiv \partial u/\partial n$). As with the boundary condition operator B, the boundary functional operator C may have different numbers of components on different parts of the boundary. The corresponding components of h may be set to zero on those parts of the boundary where the functional does not have a boundary integral contribution.

The corresponding linear adjoint problem is

$$L^* v = g,$$

in Ω, subject to the boundary conditions

$$B^* v = h,$$

on the boundary $\partial\Omega$. The fundamental identity defining L^*, B^* and the boundary operator C^* is

$$(v, Lu) + (C^*v, Bu)_{\partial\Omega} = (L^*v, u) + (B^*v, Cu)_{\partial\Omega}$$

for all u, v. This identity is obtained using integration by parts and it implies that the primal functional operator C and the adjoint boundary condition operator B^* contain an equal number of components at any location on the boundary. The construction of the appropriate adjoint operators for the linearized Euler and Navier–Stokes equations is described elsewhere [43–45].

Using the adjoint identity, the equivalent dual form of the functional is

$$J = (v, f) + (C^*v, e)_{\partial\Omega}.$$

Given approximate reconstructed solutions u_h and v_h, the error in the functional may be expressed

$$\begin{aligned}
&(g, u_h) + (h, Cu_h)_{\partial\Omega} - (g, u) - (h, Cu)_{\partial\Omega} \\
&\quad = (L^*v_h, u_h - u) + (B^*v_h, C(u_h - u))_{\partial\Omega} - (L^*v_h - g, u_h - u) - (B^*v_h - h, C(u_h - u))_{\partial\Omega} \\
&\quad = (v_h, L(u_h - u)) + (C^*v_h, B(u_h - u))_{\partial\Omega} - (L^*(v_h - v), u_h - u) - (B^*(v_h - v), C(u_h - u))_{\partial\Omega} \\
&\quad = (v_h, Lu_h - f) + (C^*v_h, Bu_h - e)_{\partial\Omega} - (v_h - v, L(u_h - u)) - (C^*(v_h - v), B(u_h - u))_{\partial\Omega}.
\end{aligned}$$

In the final result, the first two terms represent computable adjoint error estimates that describe the influence of the bulk and boundary residuals on the functional of interest. These terms may either be used to obtain a more accurate solution or to provide an asymptotically sharp bound on the error in the original functional estimate. The last two terms describe the higher order remaining error.

3.2. Defect error estimates

In general, both bulk and boundary defect corrections are required

$$L_h \Delta U_h = T_h(f - Lu_h),$$
$$B_h \Delta U_h = T_h^{\partial\Omega}(e - Bu_h),$$

driven by the bulk and boundary residuals evaluated based on the reconstructed solution u_h. Here, $T_h^{\partial\Omega}$ is a boundary transfer operator that averages the reconstructed boundary residual to form a source term for the discrete boundary conditions. Note that in the previous 1D example, the Dirichlet boundary conditions were satisfied exactly at the end points of the domain so no boundary defect iteration was needed.

4. Nonlinear formulation

This section describes the extension of the linear theory to nonlinear operators and functionals with inhomogeneous boundary conditions and functionals [3,5]. It begins with some definitions and observations regarding the linearization of functions and operators.

4.1. Preliminaries

If u is a scalar variable and $f(u)$ is a nonlinear scalar function, then a standard Taylor series expansion gives

$$f(u_2) = f(u_1) + f'(u_1)(u_2 - u_1) + \mathrm{O}((u_2 - u_1)^2).$$

Alternatively, an exact expression without remainder terms is obtained by starting from

$$\frac{\mathrm{d}}{\mathrm{d}\theta} f(u_1 + \theta(u_2 - u_1)) = f'(u_1 + \theta(u_2 - u_1))(u_2 - u_1),$$

and then integrating from $\theta = 0$ to $\theta = 1$ to give

$$f(u_2) - f(u_1) = \overline{f'}_{(u_1,u_2)}(u_2 - u_1),$$

where

$$\overline{f'}_{(u_1,u_2)} \equiv \int_0^1 f'(u_1 + \theta(u_2 - u_1))\mathrm{d}\theta.$$

For the nonlinear operator $N(u)$, the corresponding linearized operator L_u is defined formally by the Fréchet derivative

$$L_u\tilde{u} \equiv \lim_{\epsilon\to 0} \frac{N(u + \epsilon\tilde{u}) - N(u)}{\epsilon}.$$

The subscript u denotes that L_u depends on the value of u around which $N(u)$ is linearized. For example, if

$$N(u) = \frac{\partial}{\partial x}\left(\frac{1}{2}u^2\right) - \nu\frac{\partial^2 u}{\partial x^2}$$

then

$$L_u\tilde{u} = \frac{\partial}{\partial x}(u\tilde{u}) - \nu\frac{\partial^2\tilde{u}}{\partial x^2}.$$

Starting from

$$\frac{\mathrm{d}}{\mathrm{d}\theta}N(u_1 + \theta(u_2 - u_1)) = L_{u_1+\theta(u_2-u_1)}(u_2 - u_1)$$

and integrating over θ we obtain

$$N(u_2) - N(u_1) = \overline{L}_{(u_1,u_2)}(u_2 - u_1),$$

where

$$\overline{L}_{(u_1,u_2)} = \int_0^1 L|_{u_1+\theta(u_2-u_1)}\mathrm{d}\theta.$$

Thus $\overline{L}_{(u_1,u_2)}$ is the average linear operator over the "path" from u_1 to u_2.

4.2. Adjoint error estimates

Let u be the solution of the nonlinear differential equation

$$N(u) = 0$$

in the domain Ω, subject to the nonlinear boundary conditions

$$D(u) = 0$$

on the boundary $\partial\Omega$.

The linear differential operators L_u and B_u are defined by the Fréchet derivatives of N and D, respectively,

$$L_u\tilde{u} \equiv \lim_{\epsilon\to 0} \frac{N(u + \epsilon\tilde{u}) - N(u)}{\epsilon}, \quad B_u\tilde{u} \equiv \lim_{\epsilon\to 0} \frac{D(u + \epsilon\tilde{u}) - D(u)}{\epsilon}.$$

It is assumed that the nonlinear functional of interest with bulk term $J(u)$ and boundary term $K(u)$ has Fréchet derivatives of the form

$$\lim_{\epsilon\to 0}\frac{J(u+\epsilon\tilde{u})-J(u)}{\epsilon}=(g(u),\tilde{u}),\quad \lim_{\epsilon\to 0}\frac{K(u+\epsilon\tilde{u})-K(u)}{\epsilon}=(h,C_u\tilde{u})_{\partial\Omega},$$

where the operator C_u may be algebraic or differential.

The corresponding linear adjoint problem is

$$L_u^* v = g(u)$$

in Ω, subject to the boundary conditions

$$B_u^* v = h$$

on the boundary $\partial\Omega$. The adjoint identity defining L_u^*, B_u^* and the boundary operator C_u^* is

$$(v,L_u\tilde{u})+(C_u^*v,B_u\tilde{u})_{\partial\Omega}=(L_u^*v,\tilde{u})+(B_u^*v,C_u\tilde{u})_{\partial\Omega} \tag{7}$$

for all $\tilde{u}, v$. This expression implies that B_u^* has the same number of components as C_u at any point on the boundary.

We now consider approximate reconstructed primal and dual solutions u_h and v_h. The error analysis that follows makes use of the quantities $L_{u_h}^* v_h$, $B_{u_h}^* v_h$, and $C_{u_h}^* v_h$, which are computable since the linear operators are defined based on u_h rather than u. The analysis also requires averaged Fréchet derivatives defined by

$$\overline{L}_{(u,u_h)}=\int_0^1 L|_{u+\theta(u_h-u)}\mathrm{d}\theta,\quad \overline{B}_{(u,u_h)}=\int_0^1 B|_{u+\theta(u_h-u)}\mathrm{d}\theta,$$
$$\overline{C}_{(u,u_h)}=\int_0^1 C|_{u+\theta(u_h-u)}\mathrm{d}\theta,\quad \overline{g}(u,u_h)=\int_0^1 g(u+\theta(u_h-u))\mathrm{d}\theta,$$

so that

$$N(u_h)-N(u)=\overline{L}_{(u,u_h)}(u_h-u),\quad D(u_h)-D(u)=\overline{B}_{(u,u_h)}(u_h-u),$$
$$J(u_h)-J(u)=(\overline{g}(u,u_h),u_h-u),\quad K(u_h)-K(u)=(h,\overline{C}_{(u,u_h)}(u_h-u))_{\partial\Omega}.$$

Adjoint error estimates may then be expressed

$$\begin{aligned}
J(u_h)+K(u_h)-J(u)-K(u) &= (\overline{g}(u,u_h),u_h-u)+(h,\overline{C}_{(u,u_h)}(u_h-u))_{\partial\Omega}\\
&= (L_{u_h}^*v_h,u_h-u)+(B_{u_h}^*v_h,C_{u_h}(u_h-u))_{\partial\Omega}-(L_{u_h}^*v_h-\overline{g}(u,u_h),u_h-u)\\
&\quad -(h,(C_{u_h}-\overline{C}_{(u,u_h)})(u_h-u))_{\partial\Omega}-(B_{u_h}^*v_h-h,C_{u_h}(u_h-u))_{\partial\Omega}\\
&= (v_h,L_{u_h}(u_h-u))+(C_{u_h}^*v_h,B_{u_h}(u_h-u))_{\partial\Omega}-(L_{u_h}^*v_h-\overline{g}(u,u_h),u_h-u)\\
&\quad -(h,(C_{u_h}-\overline{C}_{(u,u_h)})(u_h-u))_{\partial\Omega}-(B_{u_h}^*v_h-h,C_{u_h}(u_h-u))_{\partial\Omega}\\
&= (v_h,\overline{L}_{(u,u_h)}(u_h-u))+(C_{u_h}^*v_h,\overline{B}_{(u,u_h)}(u_h-u))_{\partial\Omega}\\
&\quad -(L_{u_h}^*v_h-\overline{g}(u,u_h),u_h-u)-(h,(C_{u_h}-\overline{C}_{(u,u_h)})(u_h-u))_{\partial\Omega}\\
&\quad -(B_{u_h}^*v_h-h,C_{u_h}(u_h-u))_{\partial\Omega}+(v_h,(L_{u_h}-\overline{L}_{(u,u_h)})(u_h-u))\\
&\quad +(C_{u_h}^*v_h,(B_{u_h}-\overline{B}_{(u,u_h)})(u_h-u))_{\partial\Omega}\\
&= (v_h,N(u_h))+(C_{u_h}^*v_h,D(u_h))_{\partial\Omega}-(L_{u_h}^*v_h-\overline{g}(u,u_h),u_h-u)\\
&\quad -(h,(C_{u_h}-\overline{C}_{(u,u_h)})(u_h-u))_{\partial\Omega}-(B_{u_h}^*v_h-h,C_{u_h}(u_h-u))_{\partial\Omega}\\
&\quad +(v_h,(L_{u_h}-\overline{L}_{(u,u_h)})(u_h-u))+(C_{u_h}^*v_h,(B_{u_h}-\overline{B}_{(u,u_h)})(u_h-u))_{\partial\Omega}.
\end{aligned}$$

In the final result, the first two terms represent adjoint error estimates describing the influence of the residual errors in satisfying the PDE and the boundary conditions. These terms may be used either to provide an asymptotically sharp bound on the error in the functional estimate or to correct the error to leading order. The other terms are the remaining errors, which include the effects of the residual errors in approximating the adjoint problem and the consequences of nonlinearity on L, B, C and g.

If the solution errors for the nonlinear primal problem and the linear adjoint problem are of the same order, and they are both sufficiently smooth that the corresponding residual errors are also of the same order, then the order of accuracy of the functional approximation after making the adjoint correction is twice the order of the primal and adjoint solutions. However, rigorous a priori and a posteriori analysis of the remaining errors is much harder than in the linear case [34].

4.3. Defect error estimates

Suppose the original nonlinear PDE has the discretization

$$N_h(U_h) = 0,$$

and the boundary conditions have the discretization

$$D_h(U_h) = 0.$$

The defect calculation has the appearance of an approximate Newton iteration

$$\begin{aligned} \frac{\partial N_h}{\partial U_h}\Delta U_h &= -T_h N(u_h), \\ \frac{\partial D_h}{\partial U_h}\Delta U_h &= -T_h^{\partial\Omega} D(u_h). \end{aligned} \tag{8}$$

Note that the right-hand sides are based on the residual errors for the bulk and boundary operators N and D acting on the reconstructed solution u_h. In the same way that T_h is a transfer operator that averages the differential residual $N(u_h)$ to provide a source term for the discrete equations, the operator $T_h^{\partial\Omega}$ is a boundary transfer operator that averages the differential boundary residual $D(u_h)$ to form a source term for the discrete boundary conditions.

If a linearized discretization has not been previously implemented, it may be more convenient to base the defect iteration on the nonlinear discretization, replacing (8) by

$$\begin{aligned} N_h(U_h + \Delta U_h) - N_h(U_h) &= -T_h N(u_h), \\ D_h(U_h + \Delta U_h) - D_h(U_h) &= -T_h^{\partial\Omega} D(u_h). \end{aligned}$$

This defect iteration can be applied more than once, but for the first iteration the above equations simplify to

$$\begin{aligned} N_h(U_h + \Delta U_h) &= -T_h N(u_h), \\ D_h(U_h + \Delta U_h) &= -T_h^{\partial\Omega} D(u_h). \end{aligned}$$

4.4. Adjoint methods for shocked flows

Non-oscillatory shock-capturing schemes have revolutionized the calculation of transonic flows, providing one-point shock structures. Unfortunately, sharp shocks introduce fundamental difficulties when

attempting to use linearization approaches to evaluate the sensitivities of functionals to solution errors. In fact, a convergent nonlinear discretization may have linear sensitivities that do not converge [33].

One solution to this problem is to approach it from the perspective of well-resolved viscous shocks. Let $u_\varepsilon \equiv (\rho, q_x, p)^{\mathrm{T}}$ be the solution of the "viscous" quasi-1D Euler equations

$$\frac{\partial}{\partial x}\begin{pmatrix} A\rho q_x \\ A\rho q_x^2 \\ A\rho q_x H \end{pmatrix} + A\frac{\partial}{\partial x}\begin{pmatrix} 0 \\ p \\ 0 \end{pmatrix} = A\varepsilon\frac{\partial^2}{\partial x^2}\begin{pmatrix} \rho \\ q_x \\ p \end{pmatrix},$$

where $A(x)$ is the duct area, ρ is the density, q_x is the velocity, p is the pressure and H is the stagnation enthalpy. This may be written symbolically as

$$N(u_\varepsilon) = \varepsilon\, S(u_\varepsilon). \tag{9}$$

In the limit $\varepsilon \to 0$, u_ε will converge to the discontinuous inviscid solution u at every point except at the shock point. If $u_{\varepsilon,h}$ is an approximation to u_ε, then the error in the computed value of the functional $J(u)$ may be split into two parts

$$J(u) - J(u_{\varepsilon,h}) = (J(u) - J(u_\varepsilon)) + (J(u_\varepsilon) - J(u_{\varepsilon,h})). \tag{10}$$

The first part is the error due to the viscosity. A matched inner and outer asymptotic analysis [46,47] reveals that for functionals such as the integrated pressure,

$$J(u_\varepsilon) = J(u) + a\varepsilon + \mathrm{O}(\varepsilon^2),$$

for some constant a. Accordingly,

$$J(u) - J(u_\varepsilon) = -\varepsilon\frac{\mathrm{d}}{\mathrm{d}\varepsilon}J(u_\varepsilon) + \mathrm{O}(\varepsilon^2),$$

where the quantity

$$\frac{\mathrm{d}}{\mathrm{d}\varepsilon}J(u_\varepsilon) = \left(g(u_\varepsilon), \frac{\mathrm{d}u_\varepsilon}{\mathrm{d}\varepsilon}\right)$$

may be evaluated by the adjoint approach since by definition, the gradient with respect to ε is based on infinitesimal perturbations to the viscous solution. Differentiating (9) with respect to ε gives

$$L_{u_\varepsilon}\frac{\mathrm{d}u_\varepsilon}{\mathrm{d}\varepsilon} = S(u_\varepsilon),$$

where L_{u_ε} is the Fréchet derivative of the nonlinear operator $N - \varepsilon\, S$. Hence,

$$\left(g(u_\varepsilon), \frac{\mathrm{d}u_\varepsilon}{\mathrm{d}\varepsilon}\right) = (v_\varepsilon, S(u_\varepsilon)),$$

assuming that the viscous adjoint solution v_ε exactly satisfies the inviscid boundary conditions. If $v_{\varepsilon,h}$ is an approximation to the viscous adjoint v_ε, then $\varepsilon(v_{\varepsilon,h}, S(u_{\varepsilon,h}))$ is an approximation to the functional error due to the viscosity.

The second part of the error in (10) is due to the approximation of the solution to the viscous equation. With a well-resolved shock, it is possible to ensure that $u_\varepsilon - u_{\varepsilon,h}$ is small, so that the resulting functional error may be approximated by the usual adjoint estimate $(v_{\varepsilon,h}, N(u_{\varepsilon,h}) - \varepsilon\, S(u_{\varepsilon,h}))$. Adding the two correction terms gives the combined adjoint error estimate

$$(v_{\varepsilon,h}, N(u_{\varepsilon,h}) - \varepsilon\, S(u_{\varepsilon,h})) + \varepsilon(v_{\varepsilon,h}, S(u_{\varepsilon,h})) = (v_{\varepsilon,h}, N(u_{\varepsilon,h})).$$

It is quite striking that the final result simplifies to the standard adjoint error approximation using the *inviscid* operator N but the "viscous" approximate solutions $u_{\varepsilon,h}$ and $v_{\varepsilon,h}$. Since the viscous operator is not applied to the reconstructed solutions, the treatment of shocked flows imposes no additional accuracy requirements on the reconstruction scheme.

We conjecture that a similar treatment may be used for contact discontinuities. In that setting, the smoothing introduced by viscosity ε leads to a functional error which is $O(\sqrt{\varepsilon})$ to leading order. Hence, the final form of the adjoint correction will not have quite such a pleasingly simple form.

5. One-dimensional results

5.1. Subsonic quasi-1D flow

We first consider subsonic quasi-1D Euler flow in a converging–diverging nozzle

$$A(x) = \begin{cases} 2, & -1 \leqslant x \leqslant -\frac{1}{2}, \\ 2 - \sin^4[\pi(x+\frac{1}{2})], & -\frac{1}{2} < x < \frac{1}{2}, \\ 2, & \frac{1}{2} \leqslant x \leqslant 1, \end{cases} \tag{11}$$

with a functional that is the integral of pressure. The flow is fully determined by specifying stagnation enthalpy ($H = 4$) and stagnation pressure ($p_0 = 2$) at the inlet and pressure ($p = 1.9$) at the exit. The numerical solution of Fig. 2(a) is computed using a second-order finite volume scheme and reconstructed using cubic spline interpolation. Integrals are evaluated using 3-point Gauss quadrature so that the numerical integration errors are $O(h^6)$ [48]. The exact geometry is employed when evaluating the flow residual.

The performance of adjoint error bounding and correction is illustrated in Fig. 2(b). The bound is sharp, containing an $O(h^4)$ error compared to the $O(h^2)$ accuracy of the functional estimate. By subtracting the leading error term, we obtain an $O(h^4)$ functional estimate. Note that the temporary excursion of the base error from the overall trend is caused by a change in the sign of the error.

The combined use of defect and adjoint error correction is illustrated in Fig. 2(c). The second-order base error is bounded by the defect error estimate, or alternatively, it is corrected to obtain fourth-order accuracy. Adjoint methods are then used to obtain a sharp bound on the fourth-order functional estimate, or alternatively, to obtain a seventh-order functional estimate. The primal solution is $O(h^4)$ and the adjoint residual is $O(h^2)$ so we expect $O(h^6)$ accuracy. The higher observed rate of convergence may be related to the choice of geometry or it may result from a cancellation effect. The seventh-order accuracy is also observed for a related asymmetrical geometry.

5.2. Shocked quasi-1D flow

We now consider the integral of pressure for shocked flow in an expanding duct. The geometry is defined by the quintic polynomial $A(x)$ that yields $A'(x) = A''(x) = 0$ at $x = 0, 1$ with $A(0) = 0.95$ and $A(1) = 1.05$. Uniform inlet and outlet sections of length 0.1 are appended to this smooth expansion. The flow and adjoint solutions are both obtained using second-order finite volume schemes. Hence, the errors in the functional resulting from viscosity and from the discretization error are both second-order.

Adjoint error correction is implemented using two adaptive meshing approaches: grid redistribution and grid refinement. Using grid redistribution, grid points are moved to better resolve regions with high gradients and/or second derivatives. Using grid refinement, extra grid points are added by sub-dividing cells to better resolve the gradients in the shock region. In this implementation, both methods use a smoothed indicator function based on the pressure gradient and the local cell size. Care was taken to ensure that the

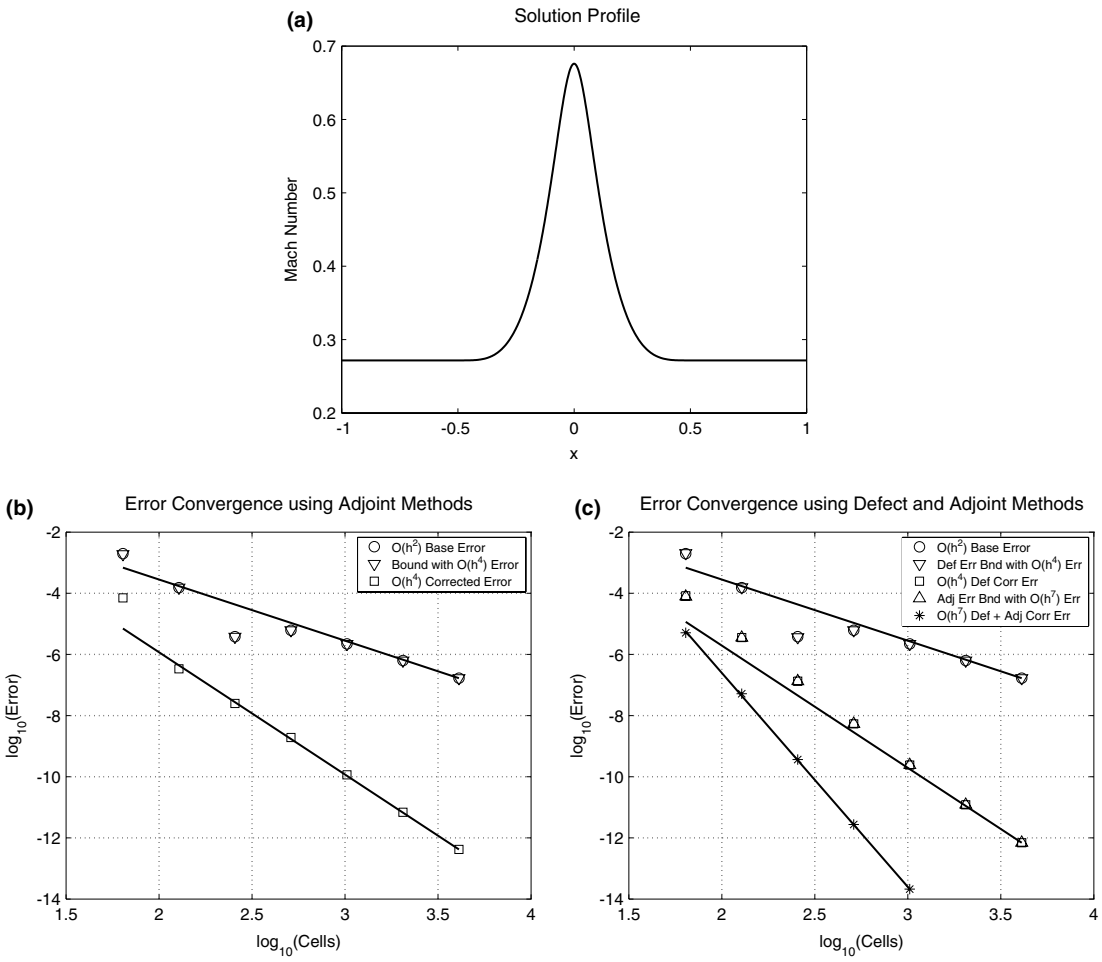

Fig. 2. Subsonic quasi-1D flow: (a) Mach number profile, (b) adjoint error bounding and correction, (c) defect error bounding and correction supplemented by adjoint error bounding and correction. The superimposed lines have slope -2, -4 or -7 as suggested by the rate descriptions in the legends.

additional numerical smoothing in the discretization of the inviscid flux terms remains second-order accurate even when there are jumps in the grid spacing. The viscous coefficient is defined by $\varepsilon = N^{-2}$, where N is the number of grid points. The effect of the grid adaptation is to smear the shock across an increasing number of grid points as N increases.

Evaluating the combined adjoint error estimates for viscous modeling error and numerical residual error, we obtain either a sharp bound on the second-order base error or a fourth-order functional estimate as seen in Fig. 3.

6. Two-dimensional implementation

6.1. Euler discretization

Steady solutions to the modified two-dimensional Euler equations satisfy the nonlinear system of PDEs

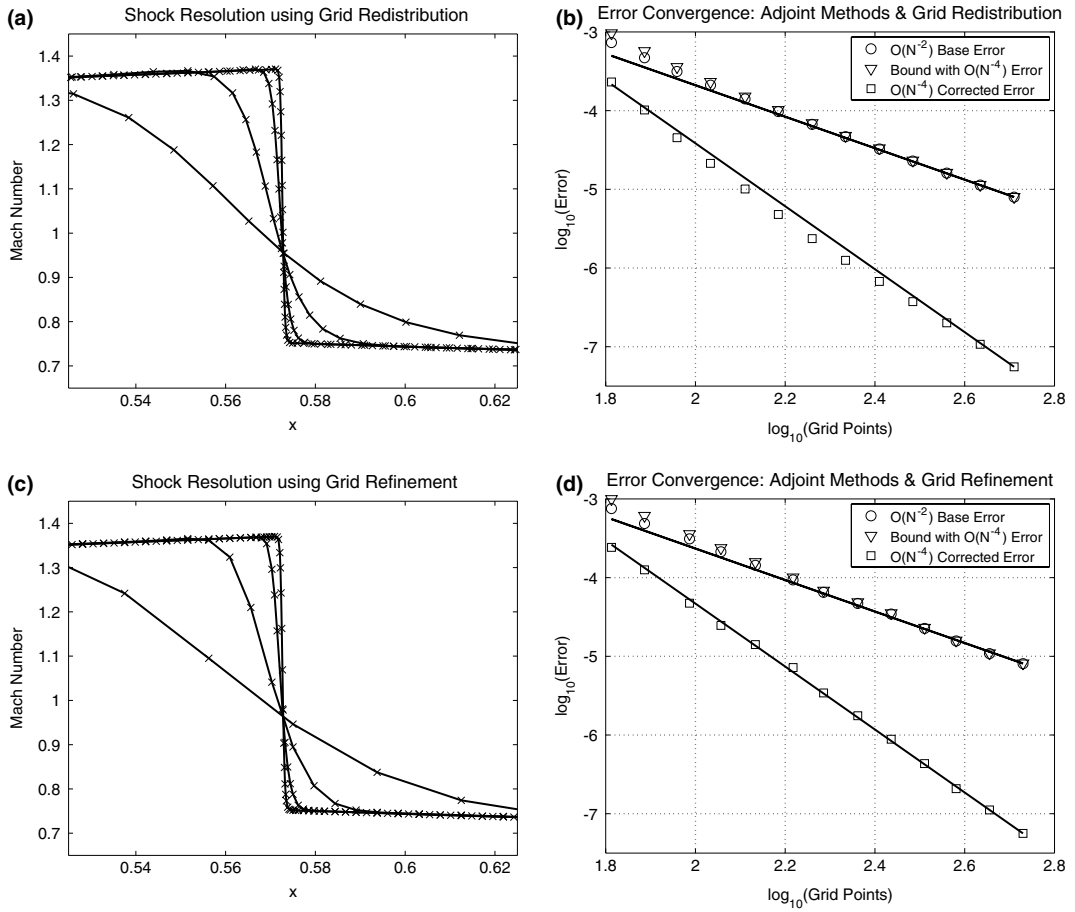

Fig. 3. Shocked quasi-1D flow. Mach number distribution on a sequence of meshes with adaptive resolution of the shock provided by (a) grid redistribution or (c) grid refinement. Adjoint error bounding and correction using cubic spline reconstruction and (b) grid redistribution or (d) grid refinement. Here, N is the number of grid points and the superimposed lines have slopes -2 and -4.

$$N(u) \equiv \frac{\partial F(u)}{\partial x} + \frac{\partial G(u)}{\partial y} - f(x,y) = 0, \tag{12}$$

where $F(u)$ and $G(u)$ are flux vectors [49], and the construction of the source term $f(x,y)$ is described in Appendix A. These equations are discretized using a cell-centered finite volume scheme with dummy cells to enforce boundary conditions. The solution is marched to a steady state using multigrid with Runge–Kutta smoothing [50,51]. Numerical dissipation scaled by the spectral radius of the flux Jacobian is based on fourth differences of the vector of conserved variables $u = (\rho, \rho q_x, \rho q_y, \rho E)^{\mathrm{T}}$. The truncation error of this scheme is $\mathrm{O}(h^2)$ in the interior of the domain.

Correct implementation of the boundary conditions is important to the order of accuracy of the functional estimates. In the description that follows, we adopt the convention that boundary normals point out of the computational domain. For the Euler equations, there is one incoming characteristic at the wall and the corresponding physical boundary condition is

$$q_n \equiv q_x n_x + q_y n_y = 0.$$

All conserved variables are linearly extrapolated to the dummy cells inside the wall so as to enforce zero normal velocity with second-order accuracy. For the duct and airfoil flows described below, reconstructed solutions based on this discretization exhibit $O(h^2)$ accuracy in the L_∞ norm.

At an inflow boundary, three physical boundary conditions and one numerical boundary condition must be specified. This is accomplished by using a Newton iteration to enforce

$$R = \begin{pmatrix} R_{\text{in}} \\ R_{\text{out}} \end{pmatrix} \equiv \begin{pmatrix} H_\infty - \bar{H} \\ s_\infty - \bar{s} \\ q_t^{ff} - \bar{q}_t \\ \Delta p + \bar{\rho}\bar{c}\Delta q_n \end{pmatrix} = 0$$

at the inflow boundary, where a bar denotes an average at the boundary of the values in the adjacent interior cell and exterior dummy cell, and Δ denotes a difference across the boundary of the values in the same two cells. The first three equations represent specification of the stagnation enthalpy, entropy and tangential velocity. For modified Euler problems, q_t^{ff} is obtained from the known analytical solution. For the duct, the equation for entropy is replaced by stagnation pressure. The fourth equation is a characteristic boundary condition on the outgoing characteristic.

At an outlet boundary, a Newton iteration is used to enforce one physical boundary condition and three numerical boundary conditions

$$R = \begin{pmatrix} R_{\text{in}} \\ R_{\text{out}} \end{pmatrix} \equiv \begin{pmatrix} p^{ff} - \bar{p} \\ \bar{c}^2\Delta\rho - \Delta p \\ \Delta q_t \\ \Delta p + \bar{\rho}\bar{c}\Delta q_n \end{pmatrix} = 0.$$

The first equation sets the exit pressure based on a far field model (e.g. the analytical solution to the modified equations) and the last three equations represent characteristic boundary conditions on the three outgoing characteristics.

6.2. Adjoint Euler equations and boundary conditions

The linearized Euler operator based on (12) is

$$L_u\tilde{u} \equiv \frac{\partial}{\partial x}\left(\frac{\partial F}{\partial u}\tilde{u}\right) + \frac{\partial}{\partial y}\left(\frac{\partial G}{\partial u}\tilde{u}\right).$$

Integrating by parts to obtain the linear adjoint operator

$$L_u^* v \equiv -\left(\frac{\partial F}{\partial u}\right)^{\mathrm{T}} \frac{\partial v}{\partial x} - \left(\frac{\partial G}{\partial u}\right)^{\mathrm{T}} \frac{\partial v}{\partial y},$$

the adjoint identity (7) is satisfied if B, C, B^*, C^* are defined on $\partial\Omega$ to satisfy

$$v^{\mathrm{T}} A_n \tilde{u} = (B^* v)^{\mathrm{T}}(C\tilde{u}) - (C^* v)^{\mathrm{T}}(B\tilde{u}) \tag{13}$$

for any $v, \tilde{u}$. Here, the operators B, C, B^*, C^* are algebraic and may be intepreted as rectangular matrices, while A_n is the normal flux Jacobian

$$A_n = \frac{\partial F}{\partial u} n_x + \frac{\partial G}{\partial u} n_y.$$

For the adjoint equations, the propagation of information along characteristics is reversed, relative to the flow equations. At the wall, there is one outgoing flow characteristic and hence one adjoint boundary

condition is required to determine the value of the incoming adjoint characteristic. Consider the typical case of a lift or drag functional where the linearized form of the nonlinear functional is $(h, \frac{\partial p}{\partial u}\tilde{u})_{\partial\Omega}$, corresponding to a weighted integral of the surface pressure distribution. It has been previously shown that the adjoint identity (13) requires the adjoint boundary condition [43]

$$B^* v \equiv v_2 n_x + v_3 n_y = h,$$

and the adjoint functional operator [44]

$$C^* v \equiv -(\rho \ \rho q_x \ \rho q_y \ \rho H) v.$$

For the inlet and outlet boundary conditions, it is convenient to express (13) in the equivalent characteristic form

$$\psi^{\mathrm{T}} \Lambda \phi = \psi^{\mathrm{T}} \begin{pmatrix} -C_\psi^* \\ B_\psi^* \end{pmatrix}^{\mathrm{T}} \begin{pmatrix} B_\phi \\ C_\phi \end{pmatrix} \phi. \tag{14}$$

Here, the characteristic adjoint and linearized flow variables are

$$\psi = T^{\mathrm{T}} v, \quad \phi = T^{-1}\tilde{u},$$

Λ is the diagonal matrix of eigenvalues of A_n, and T is the matrix of right eigenvectors of A_n.

Partitioning ϕ into incoming and outgoing flow components, the linearized far-field boundary conditions are

$$B_\phi \phi \equiv B_{\mathrm{in}} \phi_{\mathrm{in}} + B_{\mathrm{out}} \phi_{\mathrm{out}} = 0,$$

where the partitioned boundary operator is

$$(B_{\mathrm{in}} | B_{\mathrm{out}}) = \frac{\partial R_{\mathrm{in}}}{\partial u} T.$$

There is no boundary functional contribution at the far field boundary so $h = 0$ and the choice $C_\phi \phi \equiv \phi_{\mathrm{out}}$ yields the simple form

$$\begin{pmatrix} B_\phi \\ C_\phi \end{pmatrix} = \begin{pmatrix} B_{\mathrm{in}} & B_{\mathrm{out}} \\ 0 & I_{\mathrm{out}} \end{pmatrix},$$

where I_{out} is an identity matrix with dimension equal to the number of outgoing characteristics. Satisfaction of the identity (14) for any ψ, ϕ then requires

$$\begin{pmatrix} -C_\psi^* \\ B_\psi^* \end{pmatrix}^{\mathrm{T}} = \Lambda \begin{pmatrix} B_{\mathrm{in}} & B_{\mathrm{out}} \\ 0 & I_{\mathrm{out}} \end{pmatrix}^{-1} = \Lambda \begin{pmatrix} B_{\mathrm{in}}^{-1} & -B_{\mathrm{in}}^{-1} B_{\mathrm{out}} \\ 0 & I_{\mathrm{out}} \end{pmatrix},$$

yielding the adjoint characteristic boundary conditions

$$B_\psi^* \psi \equiv \Lambda_{\mathrm{out}} \psi_{\mathrm{in}} - B_{\mathrm{out}}^{\mathrm{T}} \left(B_{\mathrm{in}}^{-1}\right)^{\mathrm{T}} \Lambda_{\mathrm{in}} \psi_{\mathrm{out}} = 0,$$

and the adjoint functional operator

$$C_\psi^* \psi \equiv -(B_{\mathrm{in}}^{-1})^{\mathrm{T}} \Lambda_{\mathrm{in}} \psi_{\mathrm{out}}.$$

Identical characteristic adjoint boundary conditions are obtained [6] by adopting the alternative viewpoint of removing the dependence of the augmented linearized functional on perturbations to the flow variables [43].

The discretization of the adjoint equations and the implementation of the boundary conditions are performed following similar approaches as for the flow equations. Again the truncation error is second-order accurate in the interior of the domain and the boundary conditions are enforced with second-order accuracy. For the duct and airfoil cases considered later, the exact adjoint solutions are not known, so it is not possible to confirm directly that the computed adjoint solutions are $O(h^2)$. Here, we use the "continuous" adjoint approach [43,52] by discretizing the analytical adjoint system and boundary conditions; the "discrete" adjoint approach [53,54] of obtaining the adjoint discretization from the primal discretization would be equally valid. In either case, the approximate adjoint solution is reconstructed before performing error correction or bounding.

6.3. Reconstruction

For the two-dimensional Euler equations, the discrete solution is computed at the cell centers of a structured quadrilateral mesh. The solution is averaged to the grid nodes prior to reconstruction so that the mesh and the solution are defined at the same locations. The approximate solutions u_h and v_h are then formed using bi-cubic spline interpolation for each component. Not-a-knot boundary conditions are employed except in cases where one of the computational coordinates is periodic [55]. The coordinate data are also splined, so that the solutions and coordinates, u_h, v_h, x_h, y_h, are all defined parametrically as functions of the two spline coordinates ξ, η. Derivatives of each component of u_h can then be evaluated by solving

$$\begin{pmatrix} \frac{\partial u_h}{\partial \xi} \\ \frac{\partial u_h}{\partial \eta} \end{pmatrix} = \begin{pmatrix} \frac{\partial x_h}{\partial \xi} & \frac{\partial y_h}{\partial \xi} \\ \frac{\partial x_h}{\partial \eta} & \frac{\partial y_h}{\partial \eta} \end{pmatrix} \begin{pmatrix} \frac{\partial u_h}{\partial x} \\ \frac{\partial u_h}{\partial y} \end{pmatrix}.$$

The adjoint and defect formulations implicitly assume that all integrals are evaluated over the correct solution domain Ω and its boundary $\partial\Omega$. However, in practice, a reconstruction scheme of order r creates a reconstructed domain Ω_h that does not coincide with Ω. Using either adjoint or defect methods, it is possible to obtain functional error estimates of $O(h^r)$ by evaluating all terms on Ω_h and ignoring the geometric errors [6]. By combining adjoint and defect approaches, it is theoretically possible to obtain error estimates that exceed the order of accuracy of the reconstruction scheme. However, it then becomes necessary to correct for the influence of the geometry errors.

Let $\boldsymbol{x}(\xi)$ be a parametric representation of the boundary $\partial\Omega$, and let $\boldsymbol{x}_h(\xi)$ be the corresponding representation of the reconstructed boundary $\partial\Omega_h$. If $\Delta\boldsymbol{x}(\xi) \equiv \boldsymbol{x}_h(\xi) - \boldsymbol{x}(\xi) = O(h^r)$, then for an arbitrary function $w(\boldsymbol{x})$,

$$w(\boldsymbol{x}(\xi)) = w(\boldsymbol{x}_h(\xi)) - (\boldsymbol{x}_h(\xi) - \boldsymbol{x}(\xi)) \cdot \nabla w + O(h^{2r}),$$

and hence

$$\int_{\partial\Omega} w(\boldsymbol{x}) \mathrm{d}s = \int (w(\boldsymbol{x}_h(\xi)) - \Delta\boldsymbol{x}(\xi) \cdot \nabla w) \left| \frac{\mathrm{d}\boldsymbol{x}}{\mathrm{d}\xi} \right| \mathrm{d}\xi + O(h^{2r}).$$

Boundary integrals may therefore be evaluated to twice the order of accuracy of the reconstruction scheme by linearly extrapolating the reconstructed solution from $\partial\Omega_h$ to $\partial\Omega$ and integrating over $\partial\Omega$.

For the boundary functionals examined in this paper, the base functional estimate $K(u_h)$, the adjoint boundary term $(C^*_{u_h} v_h, D(u_h))_{\partial\Omega}$ and the defect boundary source term $T_h^{\partial\Omega} D(u_h)$ are all evaluated on the exact geometry using 3-point Gauss quadrature and linearly extrapolated values of u_h and v_h. The transfer operator $T_h^{\partial\Omega}$ is defined to be the average over the portion of $\partial\Omega$ approximated by one cell face. It is interesting to note that for a zero flux boundary condition at a solid wall, the boundary defect iteration enforces nonzero fluxes at the mesh points in order to increase the order of accuracy in satisfying zero flux on the exact geometry.

For problems with boundary functionals, it is not necessary to evaluate the bulk adjoint term $(v_h, N(u_h))$ and the bulk defect source term $T_h N(u_h)$ on the exact geometry in order to obtain error estimates with accuracy greater than the reconstruction scheme. The reason is that the only errors introduced by using the reconstructed geometry correspond to the slivers neglected between Ω and Ω_h. However, the total area of these slivers is $O(h^r)$ and the quantities being integrated are both $O(h^{\min(p,r-n)})$, so the error introduced by neglecting the slivers is $O(h^{r+\min(p,r-n)})$. This is the same order of accuracy that we expect to achieve by combining defect and adjoint methods, so no special treatment is required. We therefore evaluate these bulk terms on the reconstructed domain in (ξ, η) coordinates using 3×3 Gauss quadrature on each cell. The defect transfer operator T_h that defines the source term at each cell center is based on the average value of the source term over the computational cell.

For problems with bulk functionals, it would be necessary to correct for the errors introduced by evaluating bulk integrals on the reconstructed geometry [34]. Otherwise, the base functional estimate would contain an error of $O(h^r)$ corresponding to the area of the neglected slivers. The adjoint and defect methods would be unable to correct for this term since it results from the geometry representation.

Note that the residuals that drive the defect iteration are based on a discrete solution defined at the grid nodes. The process of averaging from the cell centers to the grid nodes may be interpreted as part of the overall second-order accurate discretization procedure. The defect iteration produces a solution at the cell centers that becomes fourth-order accurate only after the discretization process is completed by again averaging to the grid nodes. This interesting property simplifies the issue of moving solution data to the nodes.

7. Two-dimensional results

7.1. Subsonic flow in a duct

We now consider adjoint and defect methods for subsonic Euler flow in a smooth 2D duct. In performing computational experiments to study error convergence, it is very helpful to work on test cases where both the functional value and the solution are known. In Appendix A, we describe a modified Euler problem for 2D duct geometries that has a known analytical solution. Briefly, q_x is defined to be the quasi-1D value in each section, q_y varies linearly in each section so as to satisfy flow tangency at the walls, and ρ and p are defined by constant entropy and stagnation enthalpy conditions. For the present studies, we consider the drag functional on the geometry used for the quasi-1D test case (11) rescaled to be twice as long. The same inlet and outlet conditions are used, with the additional restriction that the flow is uniform at the inlet ($q_y = 0$). Starting from a structured mesh with 1024×512 cells, a sequence of coarser test meshes is obtained by removing alternate mesh points in both coordinate directions. Fig. 4(a) depicts a sample computational mesh, computed pressure and entropy contours, and residual contours obtained by substituting the reconstructed solution into the first component of the modified Euler equations.

The baseline drag estimate is $O(h^3)$ for this problem, as illustrated in Fig. 4(b). Adjoint methods provide either a sharp bound that is in error by $O(h^{5.5})$, or else an $O(h^{5.5})$ functional estimate. The numerical discretization provides $O(h^2)$ primal and dual solutions and cubic spline reconstruction provides a residual with the same order of accuracy. Hence we expect at least second order functional accuracy before correction and fourth-order accuracy after correction. In the present setting, we observe additional accuracy in each case.

A combination of defect and adjoint methods are presented for this 2D duct flow in Fig. 4(c). Defect methods provide an error estimate that is used either to provide a sharp bound on the $O(h^3)$ baseline error or subtracted to obtain an $O(h^{5.5})$ functional estimate. Adjoint methods then provide a bound on the $O(h^{5.5})$ defect estimate or else produce an $O(h^{7.5})$ functional estimate. In theory, the primal solution after defect correction should be fourth-order and the adjoint residual should be second-order so we expect sixth-order functional accuracy using the combined approach. Again, we observe additional accuracy.

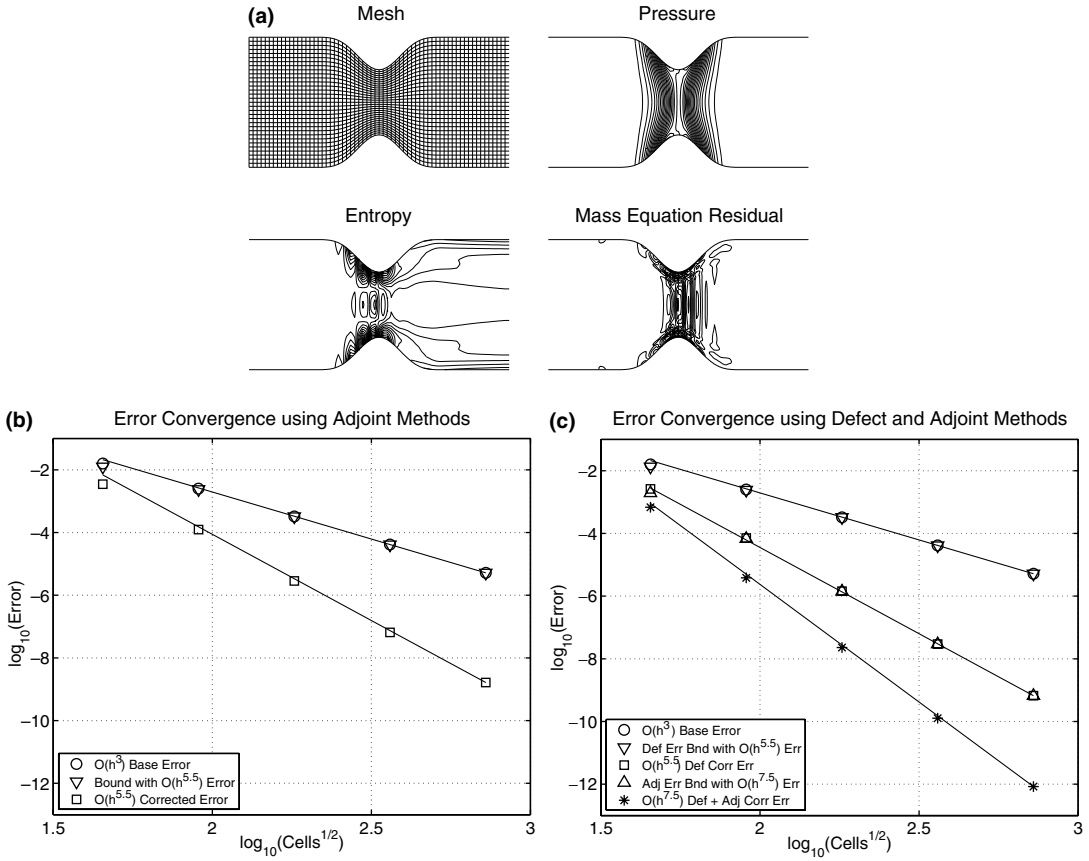

Fig. 4. Subsonic 2D flow in a duct: (a) computational mesh, computed pressure and entropy, and reconstructed mass equation residual, (b) Adjoint error bounding and correction, (c) defect error bounding and correction supplemented by adjoint error bounding and correction. The superimposed lines have slope -3, -5.5 or -7.5 as suggested by the rate descriptions in the legends.

The computational cost of adjoint error correction or bounding is approximately twice that of the original functional estimate owing to the need to solve the corresponding linear adjoint problem in addition to solving the nonlinear primal problem. Likewise, using a single primal defect iteratiaon, the cost of error correction or bounding is approximately twice that of the original functional estimate. The joint use of adjoint and defect methods leads to an algorithm that is approximately three times as expensive as the original primal calculation. In each case, the cost of reconstruction is negligible compared to the cost of solving the PDEs.

7.2. Subsonic lifting flow over an airfoil

Our final test case examines the drag for lifting flow over a Joukowski airfoil with free stream Mach number $M_\infty = 0.5$ and angle of attack $\alpha = 3°$. For this geometry, we construct a modified Euler problem with a known analytical solution. Constant entropy and stagnation enthalpy conditions are combined with a velocity field derived from the potential flow solution for the same geometry. The exact drag is non-zero for the modified solution owing to the effects of the small forcing terms in the modified equation. The computational domain is truncated at approximately 27 chords, where the far field boundary conditions are

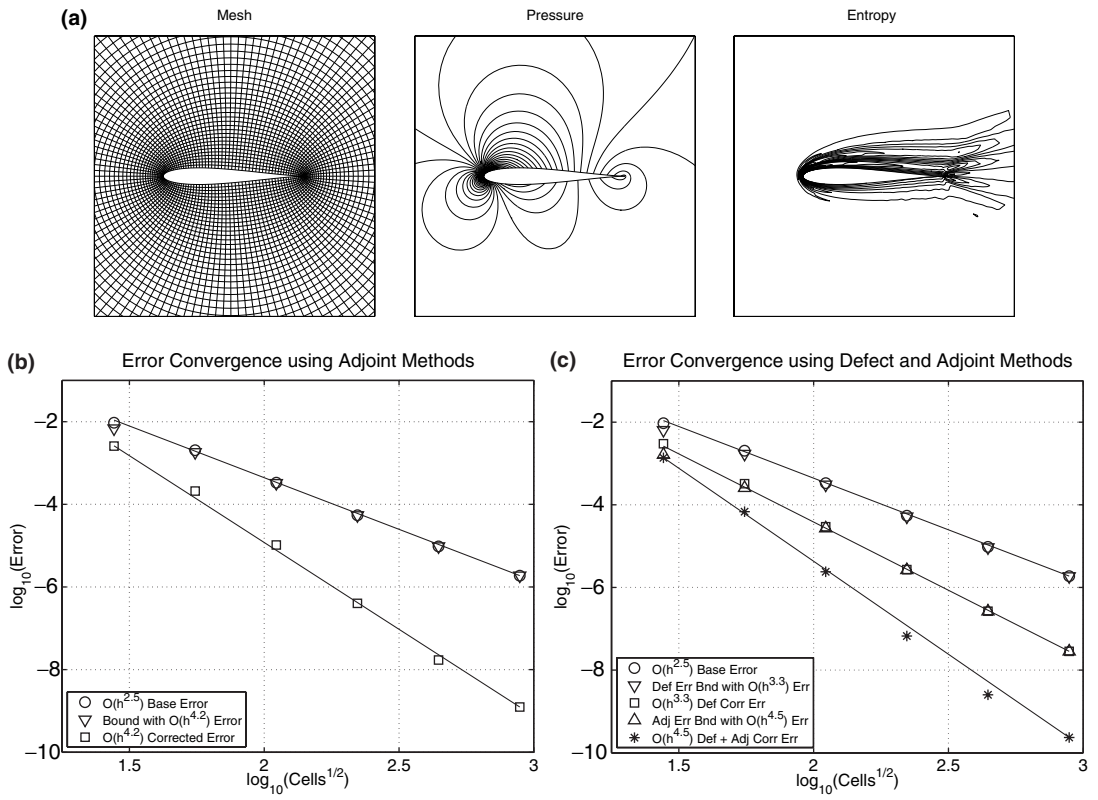

Fig. 5. Subsonic flow over a lifting airfoil: (a) computational mesh, computed pressure and entropy, (b) adjoint error bounding and correction, (c) defect error bounding and correction supplemented by adjoint error bounding and correction. The superimposed lines have slope -2.5, -3.3, -4.2 or -4.5 as suggested by the rate descriptions in the legends.

based on the exact solution to the modified Euler problem. A sequence of test meshes is obtained by isotropic coarsening of a structured 1024×768 mesh. A sample computational mesh and corresponding pressure and entropy contours are depicted in Fig. 5(a). This problem is more challenging than the smooth 2D duct, since it contains a geometric singularity at the cusped trailing edge. This singularity leads to a loss of smoothness in the reconstructed residuals near the trailing edge, invalidating error estimates of the type (1) that underlie our expectation for the order of superconvergence of the scheme.

In Fig. 5(b), we observe a base error in the drag that is $O(h^{2.5})$. The adjoint error estimate provides either an asymptotically sharp bound or a corrected functional estimate with $O(h^{4.2})$ accuracy. Alternatively, in Fig. 5(c), defect methods yield a sharp bound or a functional estimate of $O(h^{3.3})$. Applying adjoint methods to the defect corrected solution, the convergence rate is somewhat uneven, corresponding to a sharp bound that is in error by roughly $O(h^{4.5})$, or else to a functional estimate of $O(h^{4.5})$.

8. Conclusions

We have described adjoint and defect methods for obtaining sharp estimates of the error in integral functionals of PDE solutions. These estimates can be used either to provide reliable error bounds, or to correct the computed values to achieve a higher order of accuracy.

The methods were demonstrated for subsonic quasi-1D flow in a duct, achieving fourth-order accuracy with either adjoint or defect correction alone, and sixth-order accuracy using both methods together. Adjoint error methods have also been extended to treat shocked flows, using a two step correction process to account for modeling and discretization errors. Fourth order accuracy is achieved for an integral of the pressure using grid adaptation for transonic quasi-1D Euler flow.

The methods have also been applied in two dimensions to subsonic Euler flow in a duct and flow over a lifting airfoil. A modified form of the Euler equations is employed to provide systems with known analytical solutions. The best accuracy is achieved using defect and adjoint methods in combination, after accounting for geometric errors introduced by the reconstruction process. Cubic splining of the coordinate data produces a reconstructed domain and boundary that differ from the true domain and boundary. For the boundary functionals examined in the present work, this difficulty may be overcome by evaluating the boundary integrals on the true boundary, using solution values extrapolated from the cubic spline boundary.

For the 2D test cases, the analytical solution to the modified problems has been used to provide an exact far field model. The issue of far field model accuracy is conceptually distinct from the sources of error treated in this paper. It may be interesting in the future to consider adjoint approaches for computing the sensitivities of functional estimates to errors in the far field model. The difficulty is that some means of assessing the error in the far field model would be required to obtain a bound or perform a correction.

The present bounding and correction methods can be extended to unstructured computational meshes by changing to an unstructured reconstruction scheme (e.g. [25]), requiring significant further research effort. Application to Reynolds-Averaged Navier–Stokes flows requires additional effort in implementing the primal and dual viscous terms and boundary conditions [45], including primal and dual treatments for the turbulence model [54]. A discrete version of the present adjoint error estimation approach has been employed successfully on unstructured meshes to drive adaptive meshing algorithms for Euler [12] and Reynolds-averaged Navier–Stokes calculations [13,14]. The use of individual cell or element error contributions to drive adaptive error control methods is often based on a "localization" of the error contribution via the triangle inequality [28]. Localization introduces a safety margin by reducing the sharpness of the bound to the degree that it eliminates cancellation effects between elements with errors of opposite sign.

It is desirable to perform a priori analysis to complement the a posteriori error estimation techniques presented here. Rigorous a priori results have been obtained for adjoint error correction in the case of a simple one-dimensional Poisson problem [34]. Further work is required to analyze multi-dimensional linear and nonlinear problems with curved boundaries. The extension of superconvergent adjoint methods to problems with multi-dimensional shocks is also an attractive area of inquiry.

Acknowledgements

This work was funded by NASA Ames Cooperative Agreement No. NCC 2-5431.

Appendix A. Modified Euler equations

A.1. Source term

The modified 2D Euler equations are

$$N(u) \equiv \frac{\partial F(u)}{\partial x} + \frac{\partial G(u)}{\partial y} - f(x,y) = 0,$$

where $F(u)$ and $G(u)$ are the usual Euler flux vectors [49]. The source term $f(x,y)$ is defined by requiring $N(u_{\text{exact}}) = 0$ for an analytically constructed flow solution u_{exact}. Thus, u_{exact} is the exact solution of the modified flow equations, providing a reference solution against which to compare the numerical solution.

The next two sections give the construction of u_{exact} for two test cases, a 2D duct and a subsonic lifting airfoil.

A.2. 2D duct

The horizontal velocity is defined to equal the velocity in a quasi-1D flow solution [49] with duct area $A(x)$. The vertical velocity component is defined to vary linearly from the upper to lower walls so as to satisfy flow tangency

$$q_y = q_x \frac{\mathrm{d}a}{\mathrm{d}x}\frac{y}{a}.$$

Here, $a(x) = \frac{1}{2}A(x)$ is the half-height of the duct and $y = 0$ is an axis of symmetry.

The pressure and density are obtained by specifying uniform stagnation enthalpy and entropy throughout the flow field. Derivatives of the flow quantities may be obtained using standard differential relations between the flow quantities and the duct variation [49].

A.3. Subsonic lifting airfoil

The velocity field is specified to correspond to incompressible flow, and is obtained by constructing a complex potential using conformal mapping [56]. Starting from the unit cylinder $|w| = 1$ in the $w = u + \mathrm{i}v$ plane, we first map to a shifted scaled cylinder in the $z = x + \mathrm{i}y$ plane centered at

$$\gamma = \varepsilon_x - \mathrm{i}\varepsilon_y, \quad \varepsilon_x, \varepsilon_y > 0,$$

with radius $R = |1 + \gamma|$. The mapping from w to z is

$$z = -\gamma + R\mathrm{e}^{\mathrm{i}\alpha}w,$$

and the inverse mapping is

$$w = R^{-1}\mathrm{e}^{-\mathrm{i}\alpha}(z + \gamma),$$

where α is the angle of attack. The cylinder in the z plane is then mapped to a Joukowski airfoil in the $c = a + \mathrm{i}b$ plane using

$$c = \frac{1}{2}(z + z^{-1})$$

with inverse mapping

$$z = c + \sqrt{c^2 - 1}.$$

The geometry mapping derivatives are given by

$$\frac{\mathrm{d}z}{\mathrm{d}w} = R\mathrm{e}^{\mathrm{i}\alpha}, \quad \frac{\mathrm{d}w}{\mathrm{d}z} = R^{-1}\mathrm{e}^{-\mathrm{i}\alpha},$$

and

$$\frac{\mathrm{d}c}{\mathrm{d}z} = \frac{1}{2}(1 - z^{-2}), \quad \frac{\mathrm{d}z}{\mathrm{d}c} = 1 + \frac{c}{\sqrt{c^2 - 1}}.$$

Care must be taken to define the branch cut for the square root to lie inside the airfoil geometry.

The trailing edge of the airfoil is at $c = 1$, which corresponds to $z = 1$ and

$$w = \mathrm{e}^{-\mathrm{i}(\alpha+\beta)}, \quad \tan\beta \equiv \frac{\varepsilon_y}{1 + \varepsilon_x}.$$

The complex potential in the w-plane is

$$\Phi = q_0(w + w^{-1}) + \mathrm{i}\Gamma \log w,$$

with q_0 being real. The Cartesian velocity components, q_a and q_b, in the c-plane are then

$$q_a - \mathrm{i}q_b = \frac{\mathrm{d}\Phi}{\mathrm{d}c} = \frac{\mathrm{d}\Phi}{\mathrm{d}w}\frac{\mathrm{d}w}{\mathrm{d}z}\frac{\mathrm{d}z}{\mathrm{d}c}. \tag{A.1}$$

Asymptotically, as $c \to \infty$, $q_a - \mathrm{i}q_b \to 2R^{-1}\mathrm{e}^{-\mathrm{i}\alpha}q_0$, so a freestream speed q_∞ at angle of attack α requires

$$q_0 = \frac{1}{2}Rq_\infty.$$

There is a critical point in the Joukowski mapping at the cusped trailing edge, where $\mathrm{d}c/\mathrm{d}z = 0$ at $c = 1$. Examining the expression for complex velocity (A.1), the Kutta condition requires that $\mathrm{d}\Phi/\mathrm{d}w = 0$ at the cusp. This corresponds to placing a stagnation point in the w plane at $w = \mathrm{e}^{-\mathrm{i}(\alpha+\beta)}$. The corresponding vortex strength leading to smooth flow at the trailing edge is

$$\Gamma = 2q_0 \sin(\alpha + \beta).$$

The velocity expression (A.1) is indeterminate at the cusped trailing edge, but the velocity at this point can be found using L'Hospital's rule

$$q_a - \mathrm{i}q_b = \left(2q_0 w^{-3} - \mathrm{i}\Gamma w^{-2}\right)\left(\frac{\mathrm{d}w}{\mathrm{d}z}\right)^2$$

with $w = \mathrm{e}^{-\mathrm{i}(\alpha+\beta)}$.

The flow derivatives are obtained from

$$\frac{\mathrm{d}^2\Phi}{\mathrm{d}c^2} = \frac{\mathrm{d}^2\Phi}{\mathrm{d}w^2}\left(\frac{\mathrm{d}w}{\mathrm{d}z}\frac{\mathrm{d}z}{\mathrm{d}c}\right)^2 + \frac{\mathrm{d}\Phi}{\mathrm{d}w}\frac{\mathrm{d}w}{\mathrm{d}z}\frac{\mathrm{d}^2z}{\mathrm{d}c^2}$$

with

$$\frac{\partial q_a}{\partial a} = -\frac{\partial q_b}{\partial b} = \mathscr{R}\left\{\frac{\mathrm{d}^2\Phi}{\mathrm{d}c^2}\right\}, \quad \frac{\partial q_b}{\partial a} = \frac{\partial q_a}{\partial b} = -\mathscr{I}\left\{\frac{\mathrm{d}^2\Phi}{\mathrm{d}c^2}\right\}.$$

The pressure and density are again obtained by specifying uniform stagnation enthalpy and entropy throughout the flow field, with values chosen to correspond to a desired free stream Mach number.

References

[1] B. Honig, A. Nicholls, Classical electrostatics in biology and chemistry, Science 268 (1995) 1144–1149.
[2] P. Monk, E. Süli, The adaptive computation of far field patterns by a posteriori error estimates of linear functionals, SIAM J. Numer. Anal. 36 (1) (1998) 251–274.

[3] M. Giles, N. Pierce, Improved lift and drag estimates using adjoint Euler equations, in: Proc. of the 14th AIAA Computational Fluid Dynamics Conference, 1999, AIAA Paper 99-3293.
[4] N. Pierce, M. Giles, Adjoint recovery of superconvergent funtionals from PDE approximations, SIAM Rev. 42 (2) (2000) 247–264.
[5] M. Giles, N. Pierce, Adjoint error correction for integral outputs, in: Lecture Notes in Computational Science & Engineering: Error Estimation and Adaptive Discretization Methods in Computational Fluid Dynamics, vol. 25, Springer, Berlin, 2002.
[6] N. Pierce, M. Giles, Adjoint and defect error bounding and correction for functional estimates, in: Proc. of the 16th AIAA Computational Fluid Dynamics Conference, 2003, AIAA Paper 03-3846.
[7] P. Zadunaisky, On the estimation of errors propagated in the numerical integration of ordinary differential equations, Numer. Math. 27 (1976) 21–40.
[8] H. Stetter, Economical global error estimation, in: R. Willoughby (Ed.), Stiff Differential Systems, Plenum Press, New York, 1974.
[9] R. Frank, The method of iterated defect-correction and its application to two-point boundary value problems, Numer. Math. 25 (1976) 409–419.
[10] K. Böhmer, Discrete Newton methods and iterated defect corrections, Numer. Math. 37 (1981) 167–192.
[11] M. Giles, Defect and adjoint error correction, in: N. Satofuka (Ed.), Computational Fluid Dynamics 2000, Springer, Berlin, 2001.
[12] D. Venditti, D. Darmofal, Grid adaptation for functional outputs: application to two-dimensional inviscid flows, J. Comput. Phys. 176 (2002) 40–69.
[13] D. Darmofal, D. Venditti, Anisotropic grid adaptation for functional outputs: application to two-dimensional viscous flows, J. Comput. Phys. 187 (2003) 22–46.
[14] M. Park, Three-dimensional turbulent RANS error correction, in: Proc. of the 16th AIAA Computational Fluid Dynamics Conference, 2003, AIAA Paper 03-3849.
[15] I. Babuška, A. Miller, The post-processing approach in the finite element method – part 1: calculation of displacements, stresses and other higher derivatives of the displacements, Int. J. Numer. Methods Eng. 20 (1984) 1085–1109.
[16] I. Babuška, A. Miller, The post-processing approach in the finite element method – part 2: the calculation of stress intensity factors, Int. J. Numer. Methods Eng. 20 (1984) 1111–1129.
[17] J. Barrett, C. Elliott, Total flux estimates for a finite-element approximation of elliptic equations, IMA J. Numer. Anal. 7 (1987) 129–148.
[18] C. Johnson, R. Rannacher, M. Boman, Numerics and hydrodynamic stability – toward error control in computational fluid dynamics, SIAM J. Numer. Anal. 32 (4) (1995) 1058–1079.
[19] M. Paraschivoiu, J. Peraire, A. Patera, A posteriori finite element bounds for linear-functional outputs of elliptic partial differential equations, Comput. Methods Appl. Mech. Eng. 150 (1-4) (1997) 289–312.
[20] J. Peraire, A. Patera, Bounds for linear-functional outputs of coercive partial differential equations: local indicators and adaptive refinement, in: P. Ladeveze, J. Oden (Eds.), New Advances in Adaptive Computational Methods in Mechanics, Elsevier, Amsterdam, 1997.
[21] J. Oden, S. Prudhomme, New approaches to error estimation and adaptivity for the Stokes and Oseen equations, Int. J. Numer. Methods Fluids 31 (1) (1999) 3–15.
[22] P. Houston, R. Rannacher, E. Süli, A posteriori error analysis for stabilised finite element approximations of transport problems, Comput. Methods Appl. Mech. Eng. 190 (11–12) (2000) 1483–1508.
[23] R. Rannacher, Adaptive Galerkin finite element methods for partial differential equations, J. Comput. Appl. Math. 1–2 (2000) 205–233.
[24] R. Becker, R. Rannacher, An optimal control approach to error control and mesh adaptation, in: A. Iserles (Ed.), Acta Numerica 2001, Cambridge University Press, London, 2001.
[25] M. Giles, E. Süli, Adjoints methods for PDEs: a posteriori error analysis and postprocessing by duality, in: A. Iserles (Ed.), Acta Numerica 2002, Cambridge University Press, London, 2002, pp. 145–236.
[26] A. Patera, J. Peraire, A general Lagrangian formulation for the computation of a posteriori finite element bounds, in: Adaptive Finite Element Approximation of Hyperbolic Problems, vol. 25, Springer, Berlin, 2002.
[27] S. Prudhomme, J. Oden, Computable error estimators and adaptive techniques for fluid flow problems, in: Adaptive Finite Element Approximation of Hyperbolic Problems, vol. 25, Springer, Berlin, 2002.
[28] E. Süli, P. Houston, Adjoint error correction for integral outputs, in: Adaptive Finite Element Approximation of Hyperbolic Problems, vol. 25, Springer, Berlin, 2002.
[29] M. Giles, N. Pierce, Analytic adjoint solutions for the quasi-one-dimensional Euler equations, J. Fluid Mech. 426 (2001) 327–345.
[30] M. Giles, N. Pierce, On the properties of solutions of the adjoint Euler equations, in: M. Baines (Ed.), Numerical Methods for Fluid Dynamics, vol. VI, ICFD, 1998.
[31] S. Ulbrich, A sensitivity and adjoint calculus for discontinuous solutions of hyperbolic conservation laws with source terms, SIAM J. Control and Optim. 41 (3) (2002) 740–797.
[32] S. Ulbrich, Adjoint-based derivative computations for the optimal control of discontinuous solutions of hyperbolic conservation laws, Systems Control Lett. 48 (3-4) (2003) 313–328.

[33] M. Giles, Discrete adjoint approximations with shocks, in: T. Hou, E. Tadmor (Eds.), Proc. of the 9th International Conference on Hyperbolic Problems, Springer, Berlin, 2003.
[34] M. Giles, N. Pierce, Analysis of adjoint error correction for superconvergent functional estimates, Oxford University Computing Laboratory Report NA 01/14, 2001.
[35] L. Fox, Some improvements in the use of relaxation methods for the solution of ordinary and partial differential equations, Proc. Roy. Soc. London A 190 (1947) 31–59.
[36] V. Pereyra, On improving an approximate solution of a functional equation by deferred corrections, Numer. Math. 8 (1966) 376–391.
[37] V. Pereyra, Iterated deferred corrections for nonlinear boundary value problems, Numer. Math. 11 (1968) 111–125.
[38] B. Lindberg, Error estimation and iterative improvement for discretization algorithms, BIT 20 (1980) 486–500.
[39] H. Stetter, The defect correction principle and discretization methods, Numer. Math. 29 (1978) 425–443.
[40] R. Skeel, A theoretical framework for proving accuracy results for deferred corrections, SIAM J. Numer. Anal. 19 (1981) 171–196.
[41] W. Hackbusch, Local defect correction method and domain decomposition techniques, in: K. Böhmer, H. Stetter (Eds.), Defect Correction Methods: Theory and Applications, Springer, Berlin, 1984, pp. 89–113.
[42] K. Böhmer, P. Hemker, H. Stetter, The defect correction approach, in: K. Böhmer, H. Stetter (Eds.), Defect Correction Methods: Theory and Applications, Springer, Berlin, 1984, pp. 1–32.
[43] A. Jameson, Optimum aerodynamic design using control theory, Comput. Fluid Dyn. Rev. 3 (1995) 495–528.
[44] M. Giles, N. Pierce, Adjoint equations in CFD: duality, boundary conditions and solution behavior, in: Proc. of the 13th Computational Fluid Dynamics Conference, Snowmass, CO, 1997, AIAA Paper 97-1850.
[45] A. Jameson, L. Martinelli, N. Pierce, Optimum aerodynamic design using the Navier–Stokes equations, Theoret. Comput. Fluid Dyn. 10 (1998) 213–237.
[46] C. Bender, S. Orszag, Advanced Mathematical Methods for Scientists and Engineers, McGraw-Hill, New York, 1978.
[47] J. Kevorkian, J. Cole, Perturbation Methods in Applied Mathetics, Applied Math Series, 34, Springer, Berlin, 1981.
[48] G. Dahlquist, A. Björck, Numerical Methods, Prentice-Hall, Englewood cliffs, NJ, 1974.
[49] H. Liepmann, A. Roshko, Elements of gas dynamics, Wiley, New York, 1957.
[50] A. Jameson, W. Schmidt, E. Turkel, Numerical solution of the Euler equations by finite volume methods using Runge–Kutta time stepping schemes, 1981, AIAA Paper 81-1259.
[51] A. Jameson, Solution of the Euler equations by a multigrid method, Appl. Math. Comput. 13 (1983) 327–356.
[52] A. Jameson, Aerodynamic design via control theory, J. Sci. Comput. 3 (1988) 233–260.
[53] J. Elliott, J. Peraire, Practical three-dimensional aerodynamic design and optimization using unstructured grids, AIAA J. 35 (1997) 1479–1485.
[54] E. Nielsen, W. Anderson, Aerodynamic design optimization on unstructured meshes using the Navier–Stokes equations, AIAA J. 37 (1999) 957–964.
[55] C. deBoor, A Practical Guide to Splines, Springer, Berlin, 2001.
[56] G. Batchelor, An Introduction to Fluid Dynamics, Cambridge University Press, London, 1967.